ISSCR

OPEN ACCESS

Epicardially secreted fibronectin drives cardiomyocyte maturation in 3D-engineered heart tissues

Lay Ping Ong,[1,2,6,*] Johannes Bargehr,[1,2,6] Vincent R. Knight-Schrijver,[1,2,6] Jonathan Lee,[1,2] Maria Colzani,[1,2] Semih Bayraktar,[1,2] William G. Bernard,[1,2] Silvia Marchiano,[3,4] Alessandro Bertero,[5] Charles E. Murry,[3,4] Laure Gambardella,[1,2,7] and Sanjay Sinha[1,2,7,*]

[1]Wellcome – MRC Cambridge Stem Cell Institute, Jeffrey Cheah Biomedical Centre, Cambridge Biomedical Campus, University of Cambridge, Puddicombe Way, CB2 0AW Cambridge, UK
[2]Division of Cardiovascular Medicine, University of Cambridge, Addenbrooke's Hospital, ACCI Level 6, Hills Road, Box 110, Cambridge CB2 0QQ, UK
[3]Departments of Laboratory Medicine & Pathology, Bioengineering, and Medicine/Cardiology, University of Washington, Seattle, WA, USA
[4]Center for Cardiovascular Biology, Institute for Stem Cell and Regenerative Medicine, University of Washington, Seattle, WA, USA
[5]Molecular Biotechnology Center, Department of Molecular Biotechnology and Health Sciences, University of Torino, Via Nizza 52, 10126 Torino, Italy
[6]These authors contributed equally
[7]These authors contributed equally
*Correspondence: lpo20@cam.ac.uk (L.P.O.), ss661@cam.ac.uk (S.S.)
https://doi.org/10.1016/j.stemcr.2023.03.002

SUMMARY

Ischemic heart failure is due to irreversible loss of cardiomyocytes. Preclinical studies showed that human pluripotent stem cell (hPSC)-derived cardiomyocytes could remuscularize infarcted hearts and improve cardiac function. However, these cardiomyocytes remained immature. Incorporating hPSC-derived epicardial cells has been shown to improve cardiomyocyte maturation, but the exact mechanisms are unknown. We posited epicardial fibronectin (FN1) as a mediator of epicardial-cardiomyocyte crosstalk and assessed its role in driving hPSC-derived cardiomyocyte maturation in 3D-engineered heart tissues (3D-EHTs). We found that the loss of FN1 with peptide inhibition F(pUR4), CRISPR-Cas9-mediated FN1 knockout, or tetracycline-inducible FN1 knockdown in 3D-EHTs resulted in immature cardiomyocytes with decreased contractile function, and inefficient Ca^{2+} handling. Conversely, when we supplemented 3D-EHTs with recombinant human FN1, we could recover hPSC-derived cardiomyocyte maturation. Finally, our RNA-sequencing analyses found FN1 within a wider paracrine network of epicardial-cardiomyocyte crosstalk, thus solidifying FN1 as a key driver of hPSC-derived cardiomyocyte maturation in 3D-EHTs.

INTRODUCTION

The global burden of heart failure is reflected by an estimated 37.7 million patients, of whom 50% will not survive the 5 years following their diagnosis (Ziaeian and Fonarow 2016; Zarrinkoub et al., 2013). A large proportion of heart failure is due to ischemic myocardial injury resulting in loss of contractile working myocardium. The only curative therapeutic option is heart transplantation, which is substantially hampered by a severe shortage of donor organs. Regenerative cardiovascular medicine has the potential to address the loss of contractile function by remuscularizing the failing heart. Indeed, transplantation of human pluripotent stem cell (hPSC)-derived CMs (CMs) results in formation of robust cardiac grafts in rodents (Laflamme et al., 2007; Shiba et al., 2013) and non-human primates (Chong et al., 2014; Shiba et al., 2016), and improves cardiac function (Liu et al., 2018). Aside from direct intramyocardial cell injection, an alternative approach is to generate 3D-engineered heart tissues (3D-EHTs) to be transplanted on the epicardial heart surface (Weinberger et al., 2016; Tiburcy et al., 2017).

Current shortcomings limiting the efficiency of hPSC-based therapeutic applications include hPSC-CM immaturity, lack of vascular supply, and limited CM proliferation following engraftment, resulting in suboptimal function

and tissue repair. The generation of cardiovascular tissues with enhanced structure and function will aid in overcoming these limitations. In this context, the epicardium is known as an essential embryonic source of cardiac fibroblasts and coronary smooth muscle cells, which contribute to the formation of the extracellular niche and the coronary vasculature, respectively (Guadix et al., 2006; Gittenberger-de Groot et al., 1998). Recently we have demonstrated that human embryonic stem cell (hESC)-derived epicardial cells (EPIs) promote hESC-CM structural and functional maturity both *in vitro* in 3D-EHTs and *in vivo* in infarcted athymic rats, improving cardiac function and graft vascularization following transplantation (Bargehr et al., 2019).

Despite directing critical parts of cardiac development (Gittenberger-de Groot et al., 1998), the epicardial-myocardial crosstalk remains largely unelucidated. An analysis of the hESC-EPI secretome has provided an initial insight into factors implicated in these regenerative processes, highlighting the potential role of fibronectin (FN1) (Bargehr et al., 2019). In zebrafish, animals capable of cardiac regeneration, epicardial FN1 is required for repair following cardiac injury (Wang et al., 2013). Furthermore, FN1 is known to regulate key processes during development and disease, including growth, proliferation, migration, and survival (Schwarzbauer and DeSimone 2011;
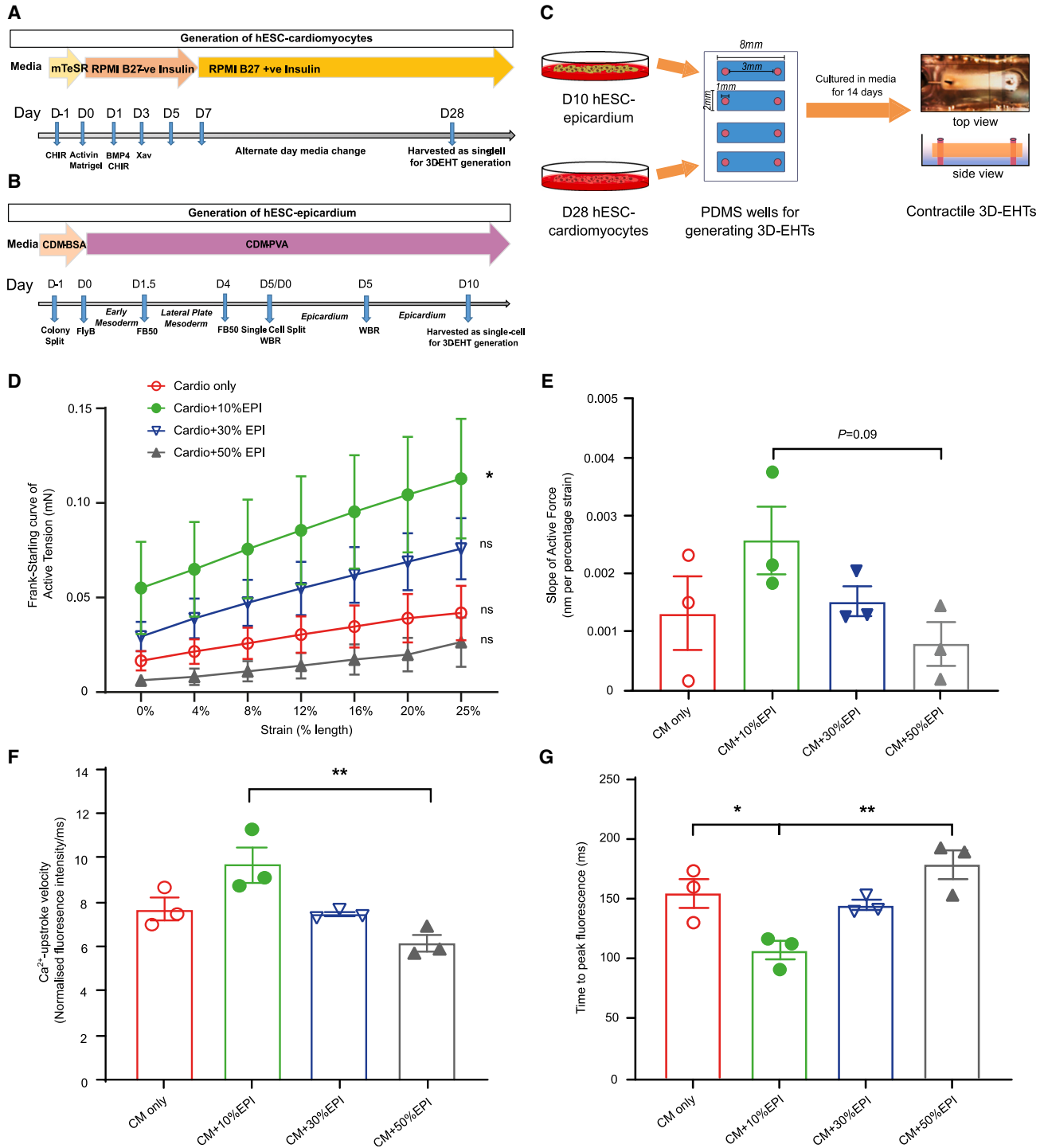
Figure 1. Generation of 3D-EHTs with optimized cell ratios

(A) Schematic for derivation of hESC-CMs.

(B) Schematic for derivation of hESC epicardium.

(C) Schematic for the generation of collagen-based 3D-EHTs containing hESC-CMs and EPIs and their subsequent histological and functional assessment.

(D) Frank-Starling curves of active force generation of 3D-EHTs containing CM only, CM + 10% hESC epicardium, CM + 30% hESC epicardium, or CM+50% hESC epicardium.

Mittal et al., 2010; Astrof et al., 2007). The embryonic identity of EPIs is critical in this process as embryonic but not adult cardiac fibroblasts can induce CM proliferation via FN1 (Ieda et al., 2009). Given the fetal identity of hESC-EPIs (Knight-Schrijver et al., 2022), we hypothesized that epicardial FN1 serves a functional role in CM development and maturation from hESCs comparable with the one seen in the developing myocardium.

Here we demonstrate the potent role of epicardial FN1 as an enhancer of CM structure and function in 3D-EHTs. We show that loss of epicardial FN1 function, first through pharmacological inhibition with pUR4, an inhibitor of FN1- integrin α5β1 binding, second through constitutive loss following CRISPR-Cas9-mediated FN1 knockout (KO), and third following tetracycline-inducible FN1 knockdown (sOPTiKD), consistently results in an impaired ability of the epicardium to promote hESC-CM maturity. A lack of epicardial FN1 deposition in 3D-EHTs results in compromised hESC-CM maturity, as demonstrated by reduced myofibril alignment, shortened sarcomeric length, impaired Ca^{2+}-kinetics, and a reduction in active force generation. To further investigate the EPI-CM crosstalk, we generate the interactome of hESC-EPI and hESC-CM using RNA bulk sequencing and reveal a unique signaling network governing myocardial growth and maturation in which FN plays a key role. These data highlight the role of FN as a key mediator of epicardial-driven growth and maturation, by assigning FN1 a vital role in the hESC-derived EPI-CM crosstalk; the analysis of which reveals signaling pathways that can be exploited to further advance regenerative cardiac applications.

RESULTS

Competitive inhibition of FN1 using the recombinant peptide pUR4 impairs hESC-CM maturation

To study the effects of epicardial FN1 on CM structure and function, we first generated 3D-EHTs with hESC-CMs and hESC-EPIs (Figures 1A–1C). For each experiment, 3D-EHTs were transferred to a myograph with a length controller and a force transducer to assess force generation followed by testing of Ca^{2+} kinetics. We also assessed CM structure using histological sections.

Before investigating the effects of FN1 inhibition, we optimized the ratio of CM and EPI cells within the 3D-EHTs and found that 3D-EHTs containing 10% EPI generated the greatest amount of active and passive force compared with 3D-EHTs containing either 30% EPI or 50% EPI, or only CM (Figures 1D, 1E, S1A, and S1B). We confirmed this result by investigating Ca^{2+} handling and found the highest Ca^{2+}-upstroke velocity, shortest time to peak, and shortest decay time in 3D-EHTs containing 10% EPI (Figures 1F, 1G, S1C, and S1D).

To test whether epicardial FN1 was at least in part responsible for the epicardial effects on CM structure and function, we inhibited FN1 using the 49-residue recombinant peptide pUR4. pUR4 binds to the N-terminal regions of FN1, competing with α5β1 for its binding domain and inhibiting assembly of FN fibrils (Figure 2A). We treated our hESC-EPI in 2D monolayers with pUR4 for 72 h and noted that FN1 protein levels in the cell/substrate layer were drastically reduced (Figure 2B). Furthermore, using immunohistochemistry (IHC) we found that FN1 deposition was qualitatively and quantitatively reduced in 3D-EHTs composed of pUR4-treated EPI cells compared with constructs containing untreated EPI (Figures 2C and 2D). This finding was consistent with diminished α5β1 clustering (Figures 2E and S1E) and paralleled by reduced sarcomeric length and myofibril alignment of CMs in 3D-EHTs containing pUR4-treated EPI (Figures 2F and 2G).

We next assessed active and passive force generation on a myograph and found that the active force generated by 3D-EHTs was significantly reduced when pUR4-treated EPI cells were used in their construction compared with untreated EPI (Figures 2H and 2I). However, pUR4-mediated inhibition of epicardial FN1 had no effect on passive force generated by 3D-EHTs (Figures 2J and 2K). Finally, we also examined Ca^{2+} handling, which showed that FN1 inhibition reduced Ca^{2+} upstroke velocity and increased times to peak fluorescent intensity of 3D-EHTs, but not decay times (Figures 2L–2O).

In summary, the performance of 3D-EHTs was impaired after inhibiting FN1-integrin binding, suggesting that intact fibrillogenesis of FN1 is an essential component of the epicardial effect on promoting structure and function of CMs.

Constitutive loss of epicardial FN1 using a CRISPR-Cas9-edited KO hESC line impairs CM maturation

To study the effects of a complete loss of epicardial FN1 from the hESC stage onwards, we generated a

(E) Slope of active force generation.
(F) Ca^{2+}-upstroke velocity of 3D-EHTs containing CM only, CM + 10% hESC epicardium, CM + 30% hESC epicardium, or CM + 50% hESC epicardium.
(G) Time to peak Ca^{2+}-fluorescence in 3D-EHTs containing CM only, CM + 10% hESC epicardium, CM + 30% hESC epicardium, or CM + 50% hESC epicardium.
(F and G) Presented calcium cycling data were taken from constructs paced at 1 Hz. Data presented as mean values; error bars represent SEM. *p < 0.05, **p < 0.005, ***p < 0.0001. Two-sided p values were calculated using a one-way ANOVA with *post hoc* correction for multiple comparisons. Each experimental group included N = 3 biological replicates.
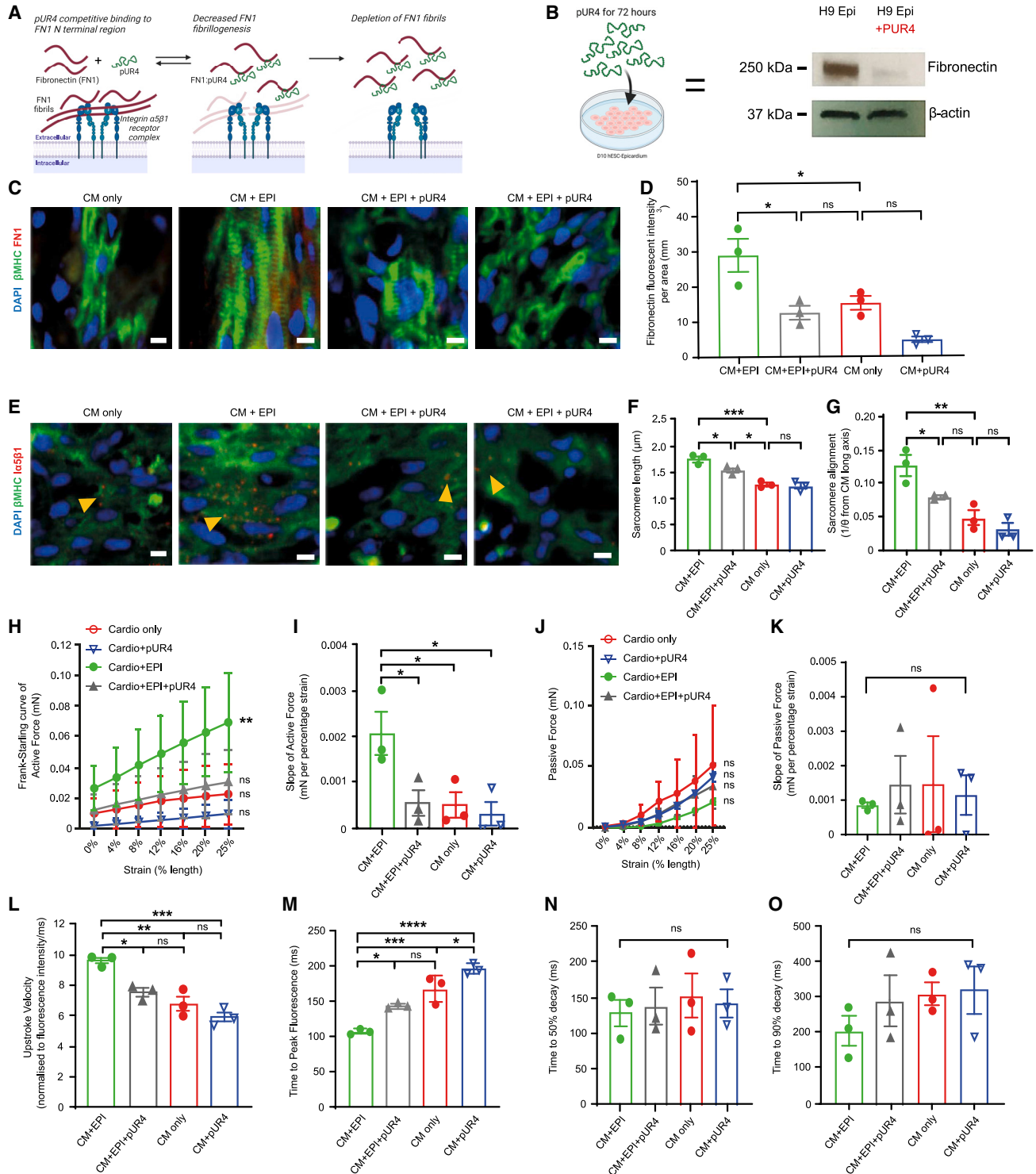
Figure 2. Pharmacological inhibition of epicardial FN1 with pUR4 results in impaired FN1 binding to integrin α5β1 and reduced CM maturation

(A) Schematic describing the mechanism of action of the recombinant peptide pUR4. PUR4 prevents FN1 from binding to the cell surface receptor integrin α5β1, hence preventing FN fibrillogenesis and signal transduction.

(B) Marked reduction of FN1 expression at the protein level 72 h post treatment of hESC epicardium with pUR4.

(legend continued on next page)

CRISPR-Cas9-edited FN1 KO line from RUES2 hESCs (KOFN1) (Figures S2A–S2C). We first showed that KOFN1-hESCs can differentiate to EPIs, as demonstrated by robust expression of the epicardial markers *WT1*, *TCF21*, and *BNC1* at the transcript and protein level, respectively (Figures 3A and 3B). At the same time KOFN1-EPI completely lacked FN1 expression both at the transcript and protein level, in contrast with wild-type (WT) EPI (Figures 3C and 3D). In 3D-EHTs containing KOFN1-EPI, FN1 deposition was also markedly reduced and clustering of integrin α5β1 was impaired (Figures 3E–3G and S2D). These results demonstrated a successful loss of FN1 in our constructs while epicardial identity was maintained, allowing us to focus on FN1-specific effects.

Using the same assessments as before, we examined how a constitutive loss of FN1 in EPI-containing 3D-EHTs affects CM structure and function. First, we found that CMs in constructs containing KOFN1-EPI had shorter sarcomeric lengths and a reduced myofibril alignment compared with CMs in constructs containing WT-EPI (Figures 3H and 3I). In line with these findings, the inclusion of KOFN1-EPI in 3D-EHTs instead of WT-EPI attenuated the active force-length relationship, while no effects on passive force generation were observed (Figures 3J–3M). This was paralleled by decreased Ca^{2+} upstroke velocity and increased time to peak fluorescence (Figures 3N and 3O), but not a significant prolongation of Ca^{2+} decay times (Figures 3P and 3Q). Finally, we noted high variance in Ca^{2+} handling data in experiments shown in Figures 1, 2, and 3 with inconsistencies in differences between the control conditions in individual experiments (hESC-CM only compared with hESC-CM + EPI) (Figures 1F, 1G, S1C, S1D, 2L–2O, 3P, and 3Q). However, we pooled the results of these control conditions together and the differences reached statistical significance, validating our experiments (Figure S4G).

Collectively, these results corroborated our findings on FN1 inhibition, demonstrating that a complete loss of epicardial FN1 in 3D-EHTs impaired CM matura-tion and produced CMs with a structure and function comparable with CMs in 3D-EHTs constructed without any EPI.

Temporal loss of epicardial FN1 expression with a tetracycline-inducible knockdown is sufficient to abrogate CM maturation

To investigate the effects of temporal modulation of epicar-dial FN1 expression, we performed a tetracycline-inducible knockdown (KD) of FN1. For this we made use of a single-step optimized inducible gene KD (sOPTiKD) of *FN1* to generate an hESC-sOPTiKD-FN1 cell line (Bertero et al., 2016, 2018) (Figures S3A–S3C). We then differentiated three sOPTiKD-FN1 H9 clones into hESC-EPI, which expressed epicardial markers including FN1 and main-tained typical epicardial morphology (Figures 4A–4C). All clones successfully downregulated *FN1* after exposure to tetracycline (up to 81%) (Figure 4B). However, we selected clone 5.3 for further experiments as it expressed the highest level of pluripotency markers at the hESC stage and epicar-dial markers after directed differentiation both with and without tetracycline (Figures S3D and S3E). We then constructed 3D-EHTs combining CMs and sOPTiKD-FN1 EPI clone 5.3 and validated our approach, finding that FN1 deposition was decreased after tetracycline exposure of 3D-EHTs containing sOPTiKD-FN1 EPI (Figures 4D, 4E, and S3F). We found that this temporal loss of FN1 following tetracycline exposure abrogated the beneficial effects caused by EPI on CM maturation and structure, including sarcomere length and alignment (Figures 4F and 4G). Addi-tionally, active force generation was reduced in 3D-EHTs containing sOPTiKD-FN1 EPI that were exposed to tetracy-cline (Figures 4H and 4I), while no effect was observed on passive force generation (Figures 4J and 4K). Furthermore, tetracycline-induced KD of FN1 resulted in increased time to peak fluorescence but had no significant impact on Ca^{2+} upstroke velocity or Ca^{2+} decay times (Figures 4L–4O).

Although these results continued to show that FN1 deposition in 3D-EHTs was a major component of the

(C–E) 3D-EHTs containing CM alone or EPI + CM, untreated or treated with pUR4. (C) Confocal images showing FN1 deposition following treatment with pUR4. Scale bar, 5 μm. (D) Quantification of FN1 following inhibition with pUR4. (E) Confocal images showing expression of integrin α5β1 following treatment with pUR4.
(F and G) Structural cardiac maturation as expressed by sarcomeric length (F) and sarcomere alignment (G) in 3D-EHTs containing CM only or CM + EPI with or without treatment with pUR4.
(H and I) Frank-Starling curves of active force generation (H) and slopes of active force (I) of 3D-EHTs containing CM only, CM + pUR4, CM + EPI, or CM + EPI + pUR4.
(J and K) Frank-Starling curves of passive force generation of 3D-EHTs containing CM only, CM + pUR4, CM + EPI, or CM + EPI + pUR4.
(L–O) Ca^{2+} kinetics of 3D-EHTs containing CM only or CM + EPI with or without treatment with pUR4. All experimental groups had N = 3 biological replicates. (L and M) Ca2+ kinetics including upstroke velocity and time to peak fluorescence of 3D-EHTs containing CM only or CM+EPI with or without treatment with pUR4. (N and O) Ca2+ kinetics including time to 50% decay and time to 90% decay of 3D-EHTs containing CM only or CM+EPI with or without treatment with pUR4. Mean values; error bars represent SEM. *p < 0.05, **p < 0.005, ***p < 0.001, ****p < 0.0001.
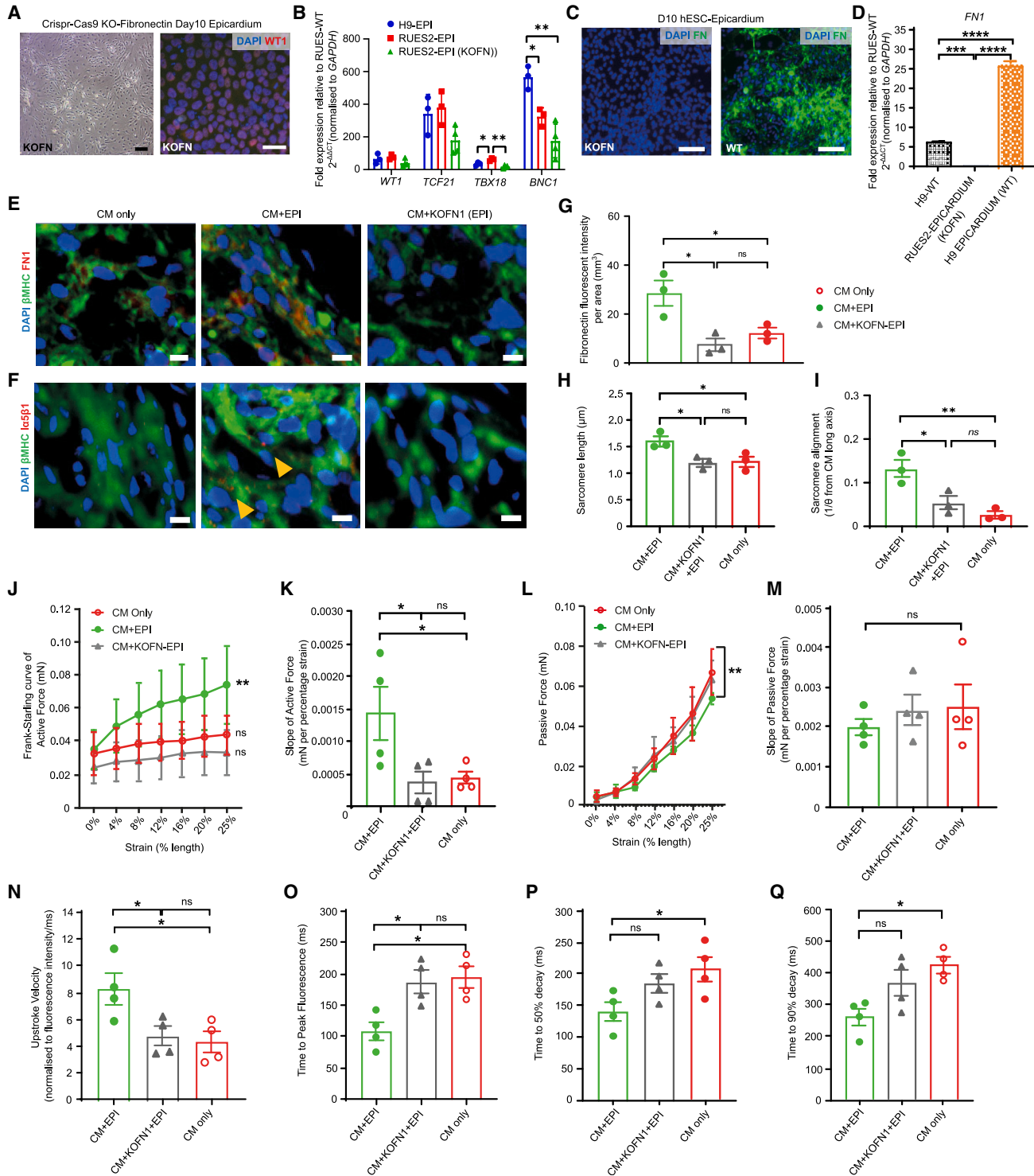
Figure 3. Constitutive loss of epicardial FN1 using a Crispr-Cas9-edited KO hESC line results in impaired CM maturation

(A) Cobblestone morphology and WT1 expression in Crispr-Cas9-edited KO FN1 epicardium. Scale bar, 20 μm.

(B) RNA expression of the key epicardial markers *WT1*, *TCF21*, *TBX18*, and *BNC1* in EPIs derived from H9-hESCs, RUES2-hESCs, and RUES2-hESC with KOFN.

(C) Confocal images showing FN1 expression in day 10 epicardium in KOFN and WT EPIs respectively. Scale bar, 50 μm.

(legend continued on next page)

epicardial effect, it was not clear if FN1 acts independently of other epicardial mechanisms. Therefore, finally we tested whether the addition of recombinant human FN1 (rhFN1) to CM-only 3D-EHTs could reproduce the effects elicited on CMs by hPSC-EPI in 3D-EHTs. We found that rhFN added to 3D-EHTs at concentrations of 10 μg/mL, 50 μg/mL, and 100 μg/m resulted in significant increases in sarcomeric length compared with untreated 3D-EHTs (Figures 5A and 5B). Moreover, improvements in sarcomere length were positively correlated with rhFN dose (one-tailed Pearson correlation; $p < 0.05$). We confirmed that FN1 was detectable in supplemented 3D-EHTs at greater levels than in 3D-EHTs without supplementation, but not at levels exceeding those seen in hESC-EPI-containing constructs (Figures 5C and 5D). Additionally, we found that 3D-EHTs treated with 100 μg/mL rhFN generated more active force than untreated 3D-EHTs, in line with hESC-EPI-containing constructs (Figures 5E and 5F). Furthermore, lower doses of rhFN also appeared to increase the passive force of 3D-EHTs (Figures 5G and 5H). However, the addition of rhFN to 3D-EHTs had no effect on Ca^{2+} handling (Figures 5I–5L).

Overall, these results provide further evidence that FN1 is required for the full positive effect of hESC-EPI on CM maturation. Moreover, by decoupling FN1 from epicardium, we have shown that FN1 may act independently to increase CM structure and function.

The EPI-CM interactome reveals a regulatory gene network driving cardiac development and regeneration

FN1 may only be one facet of EPI-CM crosstalk that regulates myocardial growth and maturation. Therefore, we investigated the interface of secreted epicardial factors and membrane-bound cell surface receptors on CMs and the role of FN1 within. To do so, we used bulk RNA-sequencing data from H9-derived hESC-EPI and hESC-CM to extract the EPI secretome and the CM membranome. A schematic of the experiment is shown in Figure 6A and the technical validation is depicted in Figure S5.

We first performed a differential expression analysis between the hESC-EPI and neural crest (NC), using DESeq2. As previously described, H9-hESC-NC was chosen as a negative control due to its redundancy in CM maturation and development (Bargehr et al., 2019). Significantly upregulated EPI genes were filtered to retain only genes encoding putatively secreted proteins according to the Human Protein Atlas (HPA) (http://www.proteinatlas.org/humanproteome/secretome) (Uhlén et al., 2019). This dataset is called the epicardial secretome (Figure 6B; Table S1). In parallel, differential expression analysis was performed between day 30 hESC-CM and H9-hESCs before differentiation. Significantly upregulated CM genes were filtered and restricted to genes encoding receptors and proteins with predicted membrane-anchored regions according to the HPA (Uhlén et al., 2019). This dataset is termed the CM membranome (Figure 6B; Table S1). In total, we found a potential secretome of 379 upregulated epicardial factors and a membranome of 1,417 upregulated CM receptors (Figure 6B; Table S1).

Next, to determine the EPI-CM interactome, these gene lists were connected, revealing a network of secreted epicardial factors and their respective membrane-bound receptors on CMs. We used the protein interaction database STRINGdb v11 (https://string-db.org/cgi/download.pl [2019 11 29]), which covered 99.5% and 95.5% of the upregulated secretome and membranome genes respectively. We constructed the interactome by filtering the secretome to retain genes that interacted with genes found only within the membranome. We then subset this list by only including interactions with a minimum experimental evidence score of above 400 for a higher confidence network (Figure 6C). Each interaction pair with a combined confidence score of above 700 was then functionally annotated following a manual literature review, categorizing the pathways where possible into the following regenerative roles: CM

(D) RNA expression of *FN1* in H9-WT, H9-EPI, and RUES2-EPI.

(E–Q) EPIs and CMs were derived from RUES2 hESC.

(E and F) Confocal images showing FN1 (E) and α5β1 expression (F) in 3D-EHTs of constructs containing CM only, CM + EPI, or CM + KOFN EPI. Scale bar, 5 μm.

(G) Quantification of FN1 expression by fluorescent intensity.

(H and I) Structural cardiac maturation as expressed by sarcomeric length (H) and sarcomere alignment (I) in 3D-EHTs containing CM only, CM + EPI, or CM + KOFN EPI.

(J and K) Frank-Starling curves of active force generation (J) and slopes of active force (K) of 3D-EHTs containing CM only, CM + EPI, or CM + KOFN EPI.

(L and M) Frank-Starling curves of passive force generation (L) and slopes of passive force (M) of 3D-EHTs containing CM only, CM + EPI, or CM + KOFN EPI.

(N–Q) Ca^{2+}-kinetics of 3D-EHTs containing CM only, CM + EPI, or KOFN EPI.

(E–Q) EPIs and CMs were derived from RUES2 hESC. All experimental groups had N = 4 biological replicates. Mean values; error bars represent SEM. *$p < 0.05$, **$p < 0.005$, ***$p < 0.001$, ****$p < 0.0001$. Two-sided p values were calculated using a one-way ANOVA with *post hoc* correction for multiple comparisons.
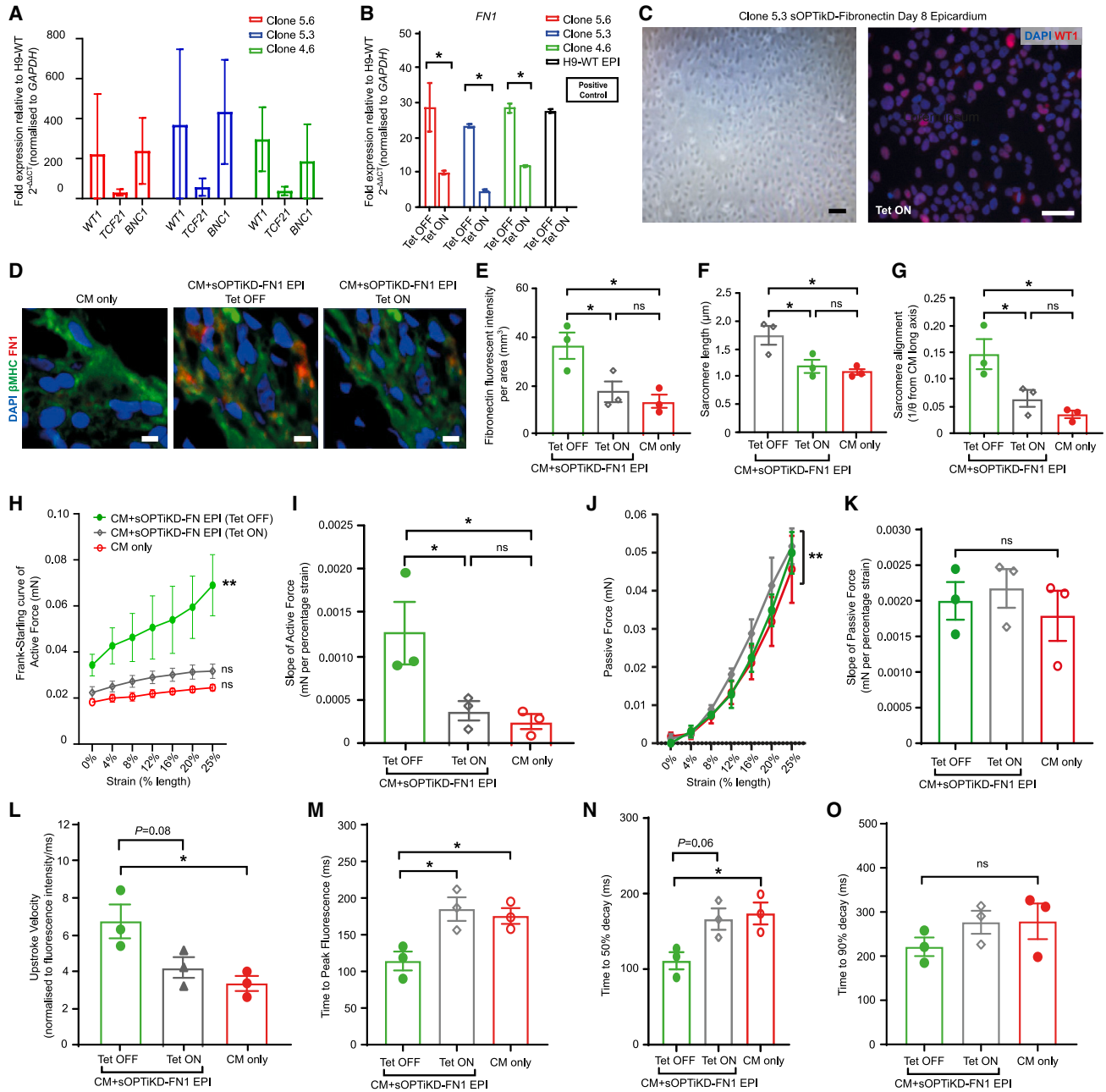
Figure 4. Temporal loss of epicardial FN1 expression with a tetracycline-inducible KD is sufficient to abrogate CM maturation

(A) RNA expression of the key epicardial markers *WT1*, *TCF21*, and *BNC1* in three sOPTiKD-FN1 clones, with the highest expression in clone 5.3.

(B) RNA expression in three sOPTiKD-FN1 clones following tetracycline exposure, with the greatest reduction in clone 5.3.

(C) Cobblestone morphology and WT1 expression in clone 5.3 differentiated to D8 hESC epicardium following 24 h of tetracycline induction. Scale bar, 20 μm.

(D) Confocal images showing FN1 expression in 3D-EHTs containing CM only, CM + sOPTiKD-FN1 EPI without tetracycline, and CM + sOPTiKD-FN1 EPI exposed to tetracycline.

(E) Quantification of FN1 expression by fluorescent intensity.

(F and G) Structural cardiac maturation as expressed by sarcomeric length (F) and sarcomere alignment (G) in 3D-EHTs containing CM only, CM + sOPTiKD-FN1 EPI without tetracycline, and CM + sOPTiKD-FN1 EPI exposed to tetracycline.

(H and I) Frank-Starling curves of active force generation (H) and slopes of active force (I) of 3D-EHTs containing CM only, CM + sOPTiKD-FN1 EPI without tetracycline, and CM + sOPTiKD-FN1 EPI exposed to tetracycline.

(legend continued on next page)

proliferation, maturation, survival, angiogenesis, development, extracellular matrix (ECM) regulation, inflammation, metabolism, and, more broadly, regeneration. Gene-pairs were then assigned to one or more of these roles (Table S1).

We found that FN1 was one component of a network of 23 predicted interactions between hESC-EPI and hESC-CM cells. Specifically, FN1 was predicted to interact in a proliferative role directly with integrins (subunits alpha 5 and beta 3) and c-MET via modulation of its ligand human growth factor, also secreted by hESC-EPI cells. Additionally, *FN1* appeared to interact with *EGFR* at the center of a hESC-CM membrane network targeted by an array of hESC-EPI factors with putative roles in ECM regulation, vasculogenesis, development, and survival among other regenerative functions (Figure 6C). Furthermore, we also predicted multiple *FN1* independent interactions between hESC-CM and hESC-EPI, including three from *RSPO1*, a recently identified regenerative epicardial protein (Li et al., 2019). Our EPI-CM interactome provides key insights into additional crosstalk between EPI and CM cells in our 3D-EHTs and presents a paracrine network that drives cardiac development and maturation in EHTs. Epicardial FN1 plays a genotypic and phenotypic key role in this process.

DISCUSSION

The addition of a stromal cell types such as the hESC-EPI to 3D-EHTs is seen to enhance hESC-CM contractile function and maturation (Bargehr et al., 2019). Although epicardial-myocardial crosstalk is likely responsible for this effect, the exact components or mechanisms governing the interaction remain unclear. Previous analysis on our 3D-EHTs placed FN1 as a likely candidate for further exploration as 3D-EHTs containing hESC-EPI had increased FN1 deposition and upregulated FN1 expression compared with hESC-NC (Bargehr et al., 2019). Here we confirm this hypothesis and provide several lines of evidence for an essential role of FN1 in improving CM maturation and function as part of the beneficial effect of hESC-EPIs as adjuvants in 3D-EHTs.
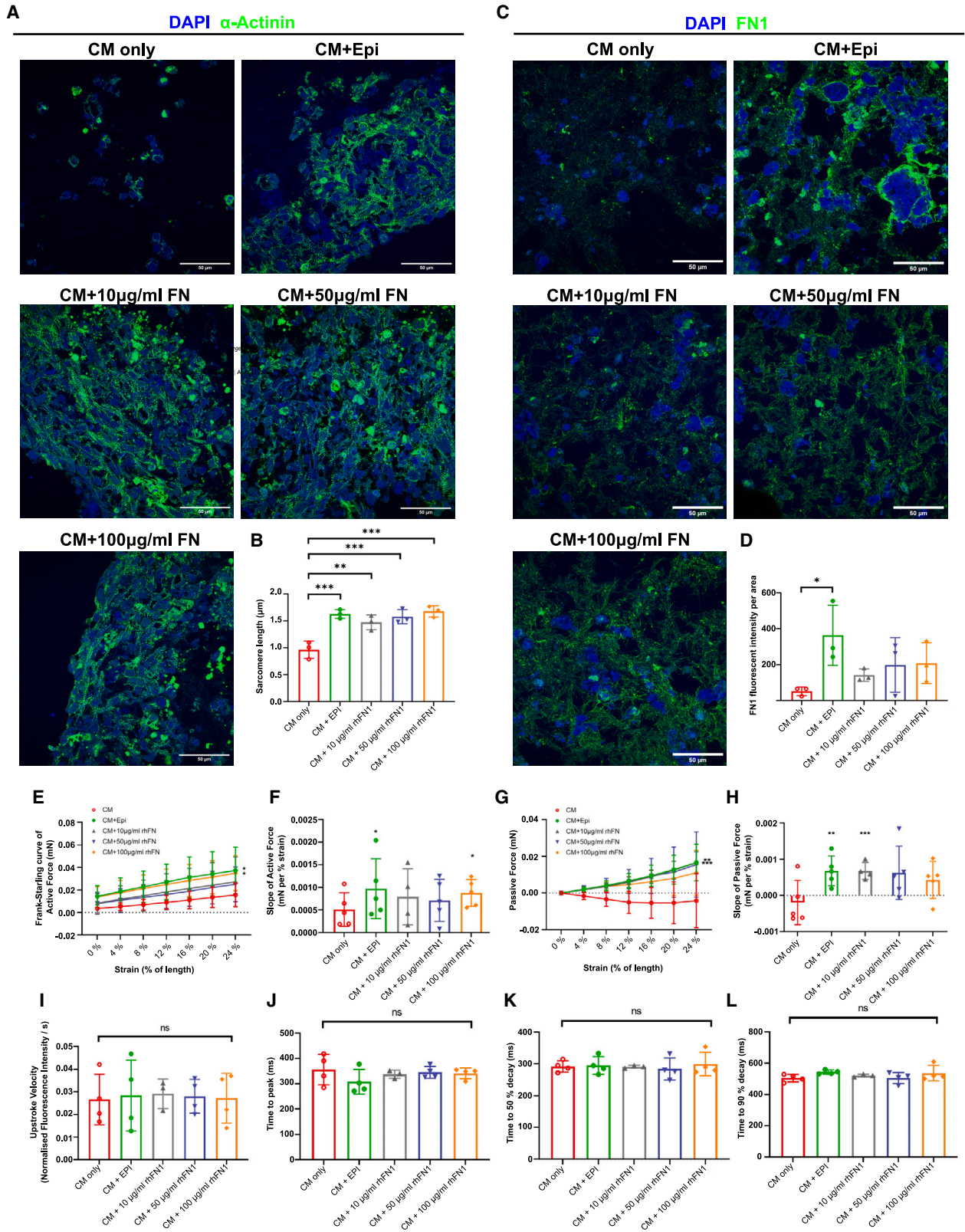
First, through histological analysis, we showed that the presence of epicardial FN1 was essential for maturation of the myofibril assembly. Without FN1, 3D-EHTs containing hESC-EPIs appeared histologically similar to those constructed with CMs alone. Second, by knocking out epicardial FN1 at both the gene and protein level, we consistently showed a loss of 3D-EHT function and

CM maturity by observing a diminished active force-length relationship and inefficient excitation-contraction coupling, which are defining features of immature CMs (Karbassi et al., 2020). Moreover, this reduced functional performance was similar to 3D-EHTs constructed with hESC-CMs only, suggesting that, without FN1, the epicardium is unable to significantly improve upon these parameters and that FN1 is necessary for the full effect of hESC-EPI in driving hESC-CM maturation in collagen-based 3D-EHTs. We demonstrated that FN1-integrin binding was the key step in this process using pUR4. Third, we were able to recapitulate structural and functional benefits of adding hESC-EPI to 3D-EHTs by supplementing rhFN into CM-only constructs. However, unlike the addition of hESC-EPI cells to 3D-EHTs, we note that rhFN administered in this manner only increased the force of CM-only constructs and not Ca^{2+} handling. While these results demonstrate that FN1 is in itself capable of augmenting 3D-EHTs and that FN1 is necessary for the full epicardial effect, they also suggest that FN1 is not the only factor in mediating the beneficial interaction between hESC-EPIs and hESC-CMs.

We attempted to explore the additional interactions between hESC-EPI and hESC-CM cells within our 3D-EHTs using bioinformatics and found FN1 in a wider paracrine interactome between both cell types. Our interactome suggests that epicardial FN1 signals via a network of receptors and soluble factors to mediate the epicardial-myocardial crosstalk. In addition to CM maturation, further downstream functions were outlined, including ECM turnover, cell survival, proliferation, and angiogenesis. Experimentally assessing the contribution of epicardial FN1 toward these additional facets of cardiac regeneration was outside of the scope of this study as 3D-EHTs restricted our observations to maturation-based observations. Nonetheless, the interactome confirmed the necessary role of epicardial FN1 within EPI-CM crosstalk and revealed other signaling effectors that may drive CM maturation that require further exploration. This list of hESC-EPI-secreted factors provides a valuable resource of targets for insight into the mechanisms that govern CM maturation. Using the interactome as a starting point, we propose that, through individual or combined perturbation, future studies may drive CM maturation using commercially available cytokines, factor-expressing microbeads, targeted genetic manipulation of the parental line, or the use of hESC-EPIs themselves, as previously described (Bargehr

(J and K) Frank-Starling curves of passive force generation (J) and slopes of passive force (K) of 3D-EHTs containing CM only, CM + sOPTiKD-FN1 EPI without tetracycline, and CM + sOPTiKD-FN1 EPI exposed to tetracycline.

(L–O) Ca^{2+} kinetics of 3D-EHTs containing CM only, CM + sOPTiKD-FN1 EPI without tetracycline, and CM + sOPTiKD-FN1 EPI exposed to tetracycline. Each experimental group included N = 3 biological replicates. Mean values; error bars represent SEM. *p < 0.05, **p < 0.005. Two-sided p values were calculated using a one-way ANOVA with *post hoc* correction for multiple comparisons.

A DAPI α-Actinin

CM only CM+Epi

CM+10μg/ml FN CM+50μg/ml FN

CM+100μg/ml FN

B

Sarcomere length (μm)

CM only
CM + EPI
CM + 10 μg/ml rhFN1
CM + 50 μg/ml rhFN1
CM + 100 μg/ml rhFN1

C DAPI FN1

CM only CM+Epi

CM+10μg/ml FN CM+50μg/ml FN

CM+100μg/ml FN

D

FN1 fluorescent intensity per area

CM only
CM + EPI
CM + 10 μg/ml rhFN1
CM + 50 μg/ml rhFN1
CM + 100 μg/ml rhFN1

E

Frank-Starling curve of Active Force (mN)

CM
CM+Epi
CM+10μg/ml rhFN
CM+50μg/ml rhFN
CM+100μg/ml rhFN

Strain (% of length)

F

Slope of Active Force (mN per % strain)

CM only
CM + EPI
CM + 10 μg/ml rhFN1
CM + 50 μg/ml rhFN1
CM + 100 μg/ml rhFN1

G

Passive Force (mN)

CM
CM+Epi
CM+10μg/ml rhFN
CM+50μg/ml rhFN
CM+100μg/ml rhFN

Strain (% of length)

H

Slope of Passive Force (mN per % strain)

CM only
CM + EPI
CM + 10 μg/ml rhFN1
CM + 50 μg/ml rhFN1
CM + 100 μg/ml rhFN1

I

Upstroke Velocity (Normalised Fluorescence Intensity / s)

ns

CM only
CM + EPI
CM + 10 μg/ml rhFN1
CM + 50 μg/ml rhFN1
CM + 100 μg/ml rhFN1

J

Time to peak (ms)

ns

CM only
CM + EPI
CM + 10 μg/ml rhFN1
CM + 50 μg/ml rhFN1
CM + 100 μg/ml rhFN1

K

Time to 50 % decay (ms)

ns

CM only
CM + EPI
CM + 10 μg/ml rhFN1
CM + 50 μg/ml rhFN1
CM + 100 μg/ml rhFN1

L

Time to 90 % decay (ms)

ns

CM only
CM + EPI
CM + 10 μg/ml rhFN1
CM + 50 μg/ml rhFN1
CM + 100 μg/ml rhFN1

et al., 2019; Iyer et al., 2015). Collectively, this interactome provides the basis to understand the beneficial effects of hESC-EPIs on structure and function of hESC-CMs by elucidating the underlying mechanistic pathways. While the epicardium is a prominent example of a cell lineage that supports cardiac development and repair, we encourage the use of these data to guide investigations on other cell types to study their regenerative function, including cardiac fibroblasts, endothelial cells, and smooth muscle cells. Code describing the derivation of the interactome is openly accessible and can be used by other groups to investigate the interaction between diverse cell types (GitHub: https://github.com/Hindrance/EpiSciData2020).

We hypothesize that a loss of FN1 impairs hESC-CM maturation through a decrease of integrin-$\alpha5\beta1$ clustering and downstream signaling as observed in this study. Normally, FN1 polymerization activates cell-surface integrin-$\alpha5\beta1$ receptors (Wickström et al. 2011; Israeli-Rosenberg et al., 2014) as an interface between extracellular and intracellular communication. Active integrins act as mechano-transducers, converting environmental mechanical cues into biochemical signals (Israeli-Rosenberg et al., 2014) that govern the cellular responses such as cell migration, survival, cell cycle progression, and differentiation (Schwarzbauer and DeSimone 2011; Wickström et al. 2011). The FN1-integrin interaction in hESC-CMs may transmit these crucial biophysical and biochemical signals for communicating environmental cues, and subsequently regulate maturation and function. We propose that the loss of epicardial FN1 impairs the ability of hESC-CMs to respond to the environment by attenuating outside-inside signaling.

Despite the wide evolutionary distance, the phenotype induced in 3D-EHTs by loss of epicardial FN1 paralleled the observations within the zebrafish. In the injured zebrafish, activated EPIs secrete FN1, which binds to integrin$\beta3$ receptors to recruit CMs within the site of injury (Wang et al., 2013). FN1 loss-of-function mutations disrupt zebrafish heart regeneration, leading to fibrosis instead of a contiguous wall of new muscle (Wang et al., 2013). We note that epicardial FN1 is highly expressed in zebrafish ECM, which may facilitate the ability of the zebrafish to successfully regenerate cardiac tissue (Mercer et al. 2013). While the dynamic nature of epicardial FN1 in human cellular models remains unclear, the role of epicardial FN1 in mediating epicardial-myocardial crosstalk to promote CM function appears to be conserved across species and broadens the relevance of our findings.

The applications for cardiac repair have grown exponentially over the past decade, ranging from direct intramyocardial injection of hPSC-derived cardiovascular cells to tissue engineering approaches and *in vitro* generation of complex tissues. While our study further highlights the complex nature of the mechanisms underlying these approaches, we have revealed one major interaction and a further network of mechanisms that may be used to optimize therapeutic approaches according to their application. For instance, tissue-engineered cardiovascular patches might prioritize the induction of vasculogenesis post transplantation over the regulation of ECM and inflammation post myocardial infarction (MI). Hence, one could selectively activate the angiogenic signaling pathways predicted by our interactome using individualized tissue constructs or microbeads that express activating factors. In contrast, for direct intramyocardial grafting of hESC-CMs, cells could be structurally and functionally matured *in vitro*, prior to transplantation targeting anti-inflammatory and pro-survival alongside ECM regulation pathways to dictate therapeutic success. Alternatively, for *in vitro* applications such as drug toxicity assays (for example, assays using chemotherapeutics to elicit toxic effects and arrhythmias), one may focus on activating cardiac maturation pathways to generate CMs with a more robust readout, more closely resembling the drug response exhibited by patients.

There were limitations within this study. Namely, experiments were carried out on small sample sizes, and biological variability was seen across all replicates when assessing force generation, Ca^{2+} handling, and sarcomeric assembly. We attribute this variability to independent cellular differentiations despite the use of robust differentiation

Figure 5. The addition of rhFN1 increases hPSC-CM maturity in 3D-EHTs without the presence of hPSC-EPI

(A) Immunofluorescent imaging of 3D-EHTs shows the arrangement of alpha-actinin within sarcomeres and localization of connexin-43 in constructs containing hPSC-CMs, hPSC-CMs + hPSC-EPIs, or hPSC-CMs + rhFN1 at varied concentrations; sarcomere lengths are quantified in (B).
(C) Immunofluorescent imaging of 3D-EHTs highlighting the quantify of FN1 and collagen deposited within constructs containing hPSC-CMs, hPSC-CMs + hPSC-EPIs, or hPSC-CMs + rhFN1 at varied concentrations; FN1 intensities are quantified in (D).
(E–H) (E) Frank-Starling curves of active force generation and (F) slopes of active force, as well as (G) curves of passive force and (H) slopes of passive force measured from 3D-EHTs containing hPSC-CMs, hPSC-CMs + hPSC-EPIs, or hPSC-CMs + rhFN1 at varied concentrations.
(I–L) Ca^{2+} kinetics of 3D-EHTs containing hPSC-CMs, hPSC-CMs + hPSC-EPIs, or hPSC-CMs + rhFN1 at varied concentrations. Each experimental group included a minimum of N = 3 biological replicates. (I and J) Ca^{2+} kinetics including upstroke velocity and time to peak fluorescence of 3D-EHTs containing hPSC-CMs, hPSC-CMs + hPSC-EPIs, or hPSC-CMs + rhFN1 at varied concentrations. (K and L) Ca2+ kinetics including time to 50% decay and time to 90% decay of 3D-EHTs containing hPSC-CMs, hPSC-CMs + hPSC-EPIs, or hPSC-CMs + rhFN1 at varied concentrations. Mean values; error bars represent SEM. *p < 0.05, **p < 0.005.
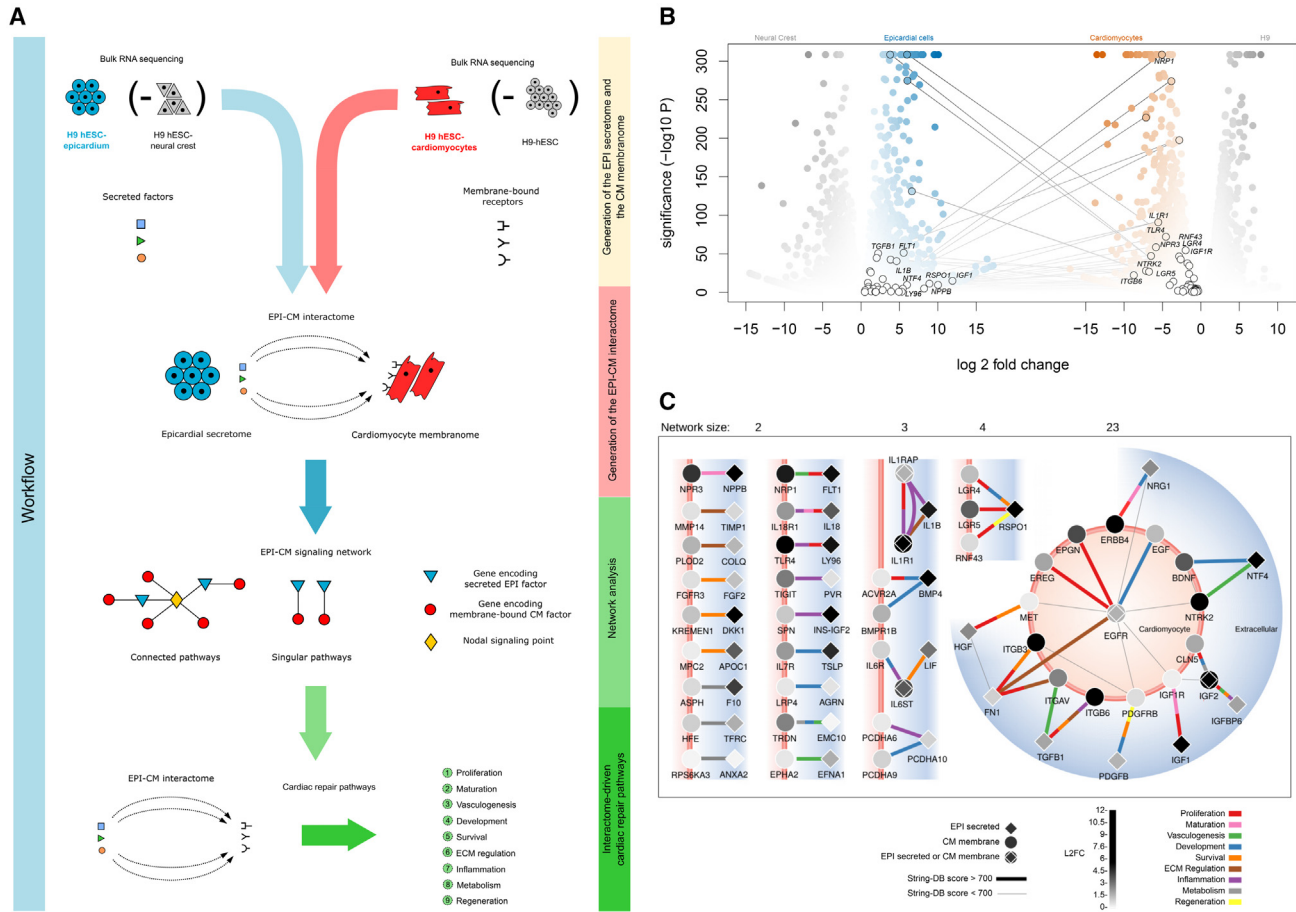
Figure 6. The EPI-CM interactome reveals a regulatory gene network driving cardiac development and regeneration

(A) Schematic overview of the study design and experimental procedure. Epicardial secretome and CM membranome were first derived using RNA sequencing. Both datasets were next integrated to generate the EPI-CM interactome, revealing a unique signaling network of regenerative pathways driving cardiac development and tissue repair. All pathways were finally ascribed reparative categories constituting a reference library for cardiac repair.

(B) The interactome between hESC-EPI secretome and hESC-CM membranome. Blue nodes on the left represent genes encoding for secreted factors expressed by hESC-EPIs compared with expression in hESC-NC, shown in gray. Orange nodes on the right depict genes encoding membrane-bound receptors expressed by hESC-CM compared with hESC. All binary hESC-EPI to hESC-CM interactions with an experimental score of above 700 in STRINGdb are shown, including a second layer of interactions formed from associations with an experimental score above 400. Respective interactions are shown with gray lines. CEPI-CM regulatory gene network driving cardiac development and regeneration.

(C) hESC-EPI-secreted genes are shown as diamond symbols on blue background, and hESC-CM membrane genes are displayed as circles on red background. Interactions with a STRINGdb score of greater than 700 are shown as bold lines and those with a STRINGdb score of less than 700 as fine lines. Strength of gene expression is expressed as L2FC and visualized by the gray tone in hESC-EPI-secreted and hESC-CM membrane gene symbols. The color of the connecting line between two genes describes the reparative category based on a manual literature review with references cited in Table S1. hESC, human embryonic stem cell; hESC-EPI, human embryonic stem cell-derived EPIs; hESC-CM, human embryonic stem cell-derived CMs; hESC-NC, human embryonic stem cell-derived neural crest cells.

protocols (Iyer et al., 2015; Bargehr et al., 2019). In particular, this affected our assessment of Ca²⁺ handling using fluorescent trace analysis as it is less sensitive than the assessment of force generation on a myograph. However, while individual Ca²⁺-handling experiments were unable to show effect size clearly, we increased statistical power by pooling the data of experiments shown in (Figures 1, 2, and 3) and demonstrated significant differences in all Ca²⁺-handling parameters between CM 3D-EHTs generated with or without hESC-EPI. Nonetheless, 3D-EHTs are the most physiologically relevant model to assess hESC-CM maturation as they enable functional readouts such as

active force-length relationship and Ca^{2+} handling (Karbassi et al., 2020). These limitations were addressed prior to experiments by ensuring that hESC-CM differentiations were pure (>80% positive for cardiac troponin T [cTNT]), and that cell viability was optimized using with a 42°C heat shock prior to constructing the 3D-EHTs. Furthermore, our hESC-EPI dose optimization experiments were performed only using hESC-EPIs derived from the H9 cell line. Although we have previously shown the benefits of hESC-EPIs on 3D-EHTs regardless of cell line (Bargehr et al., 2019), we admit that modest cell-line-dependent differences might exist at different hESC-EPI fractions. As such, the dose-response curves generated to optimize hESC-EPI content could be taken in the context of the cell line used and assessed during subsequent experiments. A final limitation is noted in the RNA-sequencing experiment that was performed on hESC derivatives *in vitro* and not from 3D-EHTs before or following transplantation. This analysis was not designed to draw conclusion about either the crosstalk between hESC-EPIs and hESC-CMs following transplantation *in vivo* or the crosstalk between primary EPIs and CMs.

To conclude, we demonstrated that FN1 promotes hESC-CM maturation and function in 3D-EHTs across a series of FN1 loss-of-function experiments and a gain-of-function experiment. Our findings implied that a loss of FN1 reduced integrin clustering and therefore signaling with hESC-CMs directed by the epicardium and epicardial FN1. Considering these results, we conclude that epicardial FN1 is necessary for mediating the full effect of hESC-EPIs in driving CM maturation in 3D-EHTs. Our epicardial-myocardial interactome expands on this key observation and highlights other components of epicardial-myocardial crosstalk that regulate proliferation, survival, angiogenesis, and ECM turnover, all processes crucial to achieving robust cardiac regeneration. Last, we conclude that our new understanding of FN1 and additional interactome may guide the development of individualized next-generation cardiac tissues for heart regeneration.

EXPERIMENTAL PROCEDURES

Resource availability

Corresponding authors
Dr. Lay Ping Ong (lpo20@cam.ac.uk) or Professor Sanjay Sinha (ss661@cam.ac.uk).

Materials availability
hESC lines used for this project are available from the corresponding authors with a completed materials transfer agreement.

Data and code availability
Data supporting the findings of this study are available within the main and supplemental manuscript. RNA-sequencing experiments are available from published datasets previously deposited in the NCBI's Gene Expression Omnibus under accession number GSE122714 for hESC-EPI and hESC-NC and GSE85331 for the hESC-CM (Liu et al., 2017) and hESC-EPI (Bargehr et al., 2019). Code generated to produce the interactome is available online (GitHub https://github.com/Hindrance/EpiSciData2020).

Differentiation of hESC-CM and hESC-EPI
EPIs were differentiated from H9 hESCs (WiCell, Madison) and from RUES2 (female line, Rockefeller University, NIH registry number 0013), respectively. The differentiation protocol was as previously described (Iyer et al., 2016). To differentiate into epicardium, cells were singly suspended in CDM-PVA, WNT3A (25 ng/mL, R&D), BMP4 (50 ng/mL), and retinoic acid (4 μM, Sigma) at a seeding density of 2.5×10^4 cells/cm^2 and replated for exactly 10 days with medium change every 5 days. CMs were differentiated from RUES2 cells as previously described (Bargehr et al., 2019) using the ABCX method (see supplemental experimental procedures). Respective karyotypes are shown in Figure S6.

Generation and characterization of 3D-EHTs
3D-EHTs were constructed in polydimethylsiloxane (PDMS) (PDMS, Sylgard 184; Dow Corning, Midland, MI) wells by combining hESC-CM and hESC-EPI in a collagen-based hydrogel as previously described (Bargehr et al., 2019).

To conduct Frank-Starling force measurements, 3D-EHTs were removed from the PDMS wells and suspended between a force transducer (Aurora Scientific, model 400A) and length controller (Aurora Scientific, model 312B). Both passive tension and active force traces were recorded and analyzed using customized LabView and MATLAB software. For non-ratiometric assessment of Ca^{2+} handling, 3D-EHTs were incubated with Fluo-4 AM (Molecular Probes, Invitrogen). Then, videos were recorded at both intrinsic contractile rates and paced at 1, 1.5, and 2 Hz before being analyzed with customized MATLAB software. Final analysis made use of Ca^{2+} data from constructs paced at 1 Hz. Representative force and Ca^{2+} traces are depicted in Figure S4. 3D-EHTs were subsequently cryo-embedded and sectioned on a cryotome prior to IHC and quantitative assessment of morphological endpoints.

Loss of function of epicardial FN
Pharmacological inhibition of epicardial FN1 with pUR4 (Genescript) was performed on day 7 of epicardial differentiation at a concentration of 500 nm for 72 h. Furthermore, 10 μL of pUR4 (500 nM) were included in the gel mixture during 3D-EHTs generation and along with medium, changed on alternate days over 14 days. FN, the protein, was subsequently quantified by western blot. The western blot technique is described in detail within supplemental experimental procedures.

To generate CRISPR-Cas9-mediated KO FN (KOFN1) hESC line, an FN1-targeted sgRNA was chosen from Genscript (https://www.genscript.com/gRNA-database.html), and cloned in pX459 (Addgene #62988 all according to a Zhang lab protocol (https://www.addgene.org/crispr/zhang/PX459-SpCas9+sgRNA). The sgRNA sequence was (5′ to 3′) CACCGTACAAACCAACGCATTGCCT with (3′ to 5′) CATGTTTGGTTGCGTAACGGACAAA. Gene targeting was done via gene juice-mediated transfection and with subsequent

genotyping of the targeted clones, as further described in the supplemental experimental procedures.

For generation of an inducible FN KD (sOPTiKD-FN1) hESC line, a short hairpin RNA (shRNA) was selected from the Broad Institute TRC library (Moffat et al., 2006). The shRNA sequences for psOP-TIkd vector construction were as follows: top (5′ to 3′) GATCCCGCCTGCTCCAAGAATTGGTTTCTCGAGAAACCAATTCT TGGAGCAGGCTTTTYTG and bottom (5′ to 3′) TCGACAAAAA AGCCTGCTCCAAGAATTGGTTTCTCGAGAAACCAATTCTTGGAG CAGGCGG. BglII overhang is in red, and terminator sequence/SalI overhang in blue.

The shRNA was into pAAV-Puro_siKD (a gift from the Vallier Group, University of Cambridge; Addgene #86695) as previously described (Bertero et al., 2016). Gene targeting was done via gene juice-mediated transfection and is described in detail in the supplemental experimental procedures along with the genotyping of the targeted clones. Differentiation of hESC epicardium was carried out in the absence of tetracycline. Tetracycline was added 2 days prior to harvest, after epicardial differentiation and maintained when 3D-EHTs were generated.

Recombinant human FN1 dose-response assay

Human plasma FN (rhFN) (Merck, F2006) was integrated into the tissue constructs at concentrations of 10, 50, and 100 μg/mL of the total tissue construct volume through subtraction of the additional sterile water volume to compensate for the volume of supplemented rhFN. After reconstitution of the cells within the gel, the tissue suspension was cast into the PDMS molds and left to solidify in the incubator at 37°C for 30 min prior to being immersed in RPMI medium supplemented with B-27 (Gibco) and insulin. The 3D-EHTs were maintained with medium changes every 2 days prior to use. Spontaneous contractions were observed within 3 days.

Bulk RNA sequencing

Starting material for RNA sequencing was composed of H9 hESC-EPI, H9 hESC-NC, and H9 hESC-CM as well as undifferentiated H9 hESCs. The datasets had previously been deposited in the NCBI's Gene Expression Omnibus under accession number GSE122714 for hESC-EPI and hESC-NC and GSE85331 for the hESC-CM (Liu et al., 2017) and hESC-EPI (Bargehr et al., 2019).

Analysis of epicardial-CM interactome

We first performed a differential expression analysis between the hESC-EPI and hESC-NC, using DESeq2. As previously described, hESC-NCs were chosen as a negative control due to their redundancy in hESC-CM maturation and development. The list of differentially upregulated genes was filtered to retain only genes encoding putatively secreted proteins according to the HPA (http://www.proteinatlas.org/humanproteome/secretome) (Uhlén et al., 2019). This dataset is called the hESC-EPI secretome. In parallel, differential expression analysis was performed between day 30 hESC-CM and H9s before differentiation. The list of differentially expressed genes was filtered and restricted to genes encoding receptors and proteins with predicted membrane-anchored regions according to the HPA (Uhlén et al., 2019). This dataset is termed the hESC-CM membranome. Next, to determine the interactome, both gene lists were jointly analyzed to elucidate hESC-EPI-secreted factors and their respective membrane-bound receptors on hESC-CMs. We used the interaction database STRINGdb v11 (https://string-db.org/cgi/download.pl [2019 11 29]), which covered 99.5% and 95.5% of the upregulated secretome and membranome genes respectively. We constructed the interactome by filtering the secretome to retain genes with interactions with genes only found in the membranome. The interactome network is shown in Figure 6 and Table S1. The technical validation of the sequenced data and EPI/CM differentiation is detailed in the supplemental experimental procedures and Figure S5, respectively.

Statistical analysis

All *in vitro* studies were performed as three parallel technical replicates for each individual biological replicate. Each biological replicate was an independent experiment with EHTs generated on different days and measured separately, from different cellular differentiations. Statistical testing was only performed on biological replicates, using an unpaired t test for two-group comparisons and a paired t test for comparison of two paired groups. One-way ANOVA was used for the statistical comparison of more than two groups, and a *post hoc* Tukey test was used if the group variance was equal. As for groups with unequal variance, a *post hoc* Kruskal-Wallis test with Dunn's correction for multiple comparisons was applied. Measuring two-sided significance, a p value of 0.05 was considered statistically significant. All results are presented as mean ± SEM unless otherwise stated. All analyses were performed using GraphPad Prism 9.0 software.

SUPPLEMENTAL INFORMATION

Supplemental information can be found online at https://doi.org/10.1016/j.stemcr.2023.03.002.

CONFLICT OF INTERESTS

S.S. and J.B. are co-founders and shareholders in ABS Biotechnologies GmbH.

REFERENCES

Astrof, S., Denise, C., and Hynes, R.O. (2007). Multiple cardiovascular defects caused by the absence of alternatively spliced segments of fibronectin. Dev. Bio. *311*, 11–24. https://doi.org/10.1016/j.ydbio.2007.07.005.

Bargehr, J., Ong, L.P., Colzani, M., Davaapil, H., Hofsteen, P., Bhandari, S., Gambardella, L., Le Novère, N., Iyer, D., Sampaziotis, F., et al. (2019). Epicardial cells derived from human embryonic stem cells augment cardiomyocyte-driven heart regeneration. Nat. Biotechnol. *37*, 895–906. https://doi.org/10.1038/s41587-019-0197-9.

Bertero, A., Pawlowski, M., Ortmann, D., Snijders, K., Yiangou, L., Cardoso De Brito, M., Brown, S., Bernard, W.G., Cooper, J.D., Giacomelli, E., et al. (2016). Optimized inducible ShRNA and CRISPR/Cas9 platforms for in vitro studies of human development using HPSCs. Development *143*, 4405–4418. https://doi.org/10.1242/dev.138081.

Bertero, A., Yiangou, L., Brown, S., Ortmann, D., Pawlowski, M., and Vallier, L. (2018). Conditional manipulation of gene function in human cells with optimized inducible ShRNA. Current Protocols in Stem Cell Biology *44*, 5C.4.1–5C.4.48. https://doi.org/10.1002/cpsc.45.

Chong, J.J.H., Yang, X., Don, C.W., Minami, E., Liu, Y.-W, Weyers, J.J., Mahoney, W.M., Van Biber, B., Cook, S.M., Palpant, N.J., et al. (2014). Human embryonic stem cell-derived cardiomyocytes regenerate non-human primate hearts. Nature *510*, 273–277. https://doi.org/10.1038/nature13233.Human.

Gittenberger-de Groot, A.C., Vrancken Peeters, M.P., Mentink, M.M., Gourdie, R.G., and Poelmann, R.E. (1998). Epicardium-derived cells contribute a novel population to the myocardial wall and the atrioventricular cushions. Circ. Res. *82*, 1043–1052. https://doi.org/10.1161/01.RES.82.10.1043.

Guadix, J.A., Carmona, R., Muñoz-Chápuli, R., and Pérez-Pomares, J.M. (2006). In vivo and in vitro analysis of the vasculogenic potential of avian proepicardial and epicardial cells. Dev. Dyn. *235*, 1014–1026. https://doi.org/10.1002/dvdy.20685.

Ieda, M., Tsuchihashi, T., Ivey, K.N., Ross, R.S., Hong, T.T., Shaw, R.M., and Srivastava, D. (2009). Cardiac fibroblasts regulate myocardial proliferation through B1 integrin signaling. Dev. Cell *16*, 233–244. https://doi.org/10.1016/j.devcel.2008.12.007.

Israeli-Rosenberg, S., Manso, A.M., Okada, H., and Ross, R.S. (2014). Integrins and integrin-associated proteins in the cardiac myocyte. Circ. Res. *114*, 572–586. https://doi.org/10.1161/CIRCRESAHA.114.301275.

Iyer, D., Gambardella, L., Bernard, W.G., et al. (2016). Robust derivation of epicardium and its differentiated smooth muscle cell progeny from human pluripotent stem cells. Development *143*, 904.

Iyer, D., Gambardella, L., Bernard, W.G., Serrano, F., Mascetti, V.L., Pedersen, R.A., Talasila, A., and Sinha, S. (2015). Robust derivation of epicardium and its differentiated smooth muscle cell progeny from human pluripotent stem cells. DevelopmentEngland *142*, 1528–1541. https://doi.org/10.1242/dev.119271.

Karbassi, E., Fenix, A., Marchiano, S., Muraoka, N., Nakamura, K., Yang, X., and Murry, C.E. (2020). Cardiomyocyte maturation: advances in knowledge and implications for regenerative medicine. Nat. Rev. Cardiol. *17*, 341–359. https://doi.org/10.1038/s41569-019-0331-x.

Knight-Schrijver, V.R., Davaapil, H., Bayraktar, S., Ross, A.D.B., Kanemaru, K., Cranley, J., Dabrowska, M., et al. (2022). A single-cell comparison of adult and fetal human epicardium defines the age-associated changes in epicardial activity. Nature Cardiovascular Research *1*, 1215–1229. https://doi.org/10.1038/s44161-022-00183-w.

Laflamme, M.A., Chen, K.Y., Naumova, A.V., Muskheli, V., Fugate, J.A., Dupras, S.K., Reinecke, H., Xu, C., Hassanipour, M., Police, S., et al. (2007). Cardiomyocytes derived from human embryonic stem cells in pro-survival factors enhance function of infarcted rat hearts. Nat. Biotechnol. *25*, 1015–1024. https://doi.org/10.1038/nbt1327.

Li, G., Tian, L., Goodyer, W., Kort, E.J., Buikema, J.W., Xu, A., Wu, J.C., Jovinge, S., and Wu, S.M. (2019). Single cell expression analysis reveals anatomical and cell cycle-dependent transcriptional shifts during heart development. Development *146*, dev173476.

Liu, Y.W., Chen, B., Yang, X., Fugate, J.A., Kalucki, F.A., Futakuchi-Tsuchida, A., Couture, L., Vogel, K.W., Astley, C.A., Baldessari, A., et al. (2018). Human embryonic stem cell-derived cardiomyocytes restore function in infarcted hearts of non-human primates. Nat. Biotechnol. *36*, 597–605. https://doi.org/10.1038/nbt.4162.

Liu, Q., Jiang, C., Xu, J., Zhao, M.T., Van Bortle, K., Cheng, X., et al. (2017). Genome-wide temporal profiling of transcriptome and open chromatin of early cardiomyocyte differentiation derived from hiPSCs and hESCs. Circ. Res. *121*, 376–391.

Mercer, S.E., Odelberg, S.J., and Simon, H.G. (2013). A dynamic spatiotemporal extracellular matrix facilitates epicardial-mediated vertebrate heart regeneration. Dev. Biol. *382*, 457–469. https://doi.org/10.1016/j.ydbio.2013.08.002.

Mittal, A., Pulina, M., Hou, S.Y., and Astrof, S. (2010). Fibronectin and integrin alpha 5 play essential roles in the development of the cardiac neural crest. Mech. Dev. *127*, 472–484. https://doi.org/10.1016/j.mod.2010.08.005.

Moffat, J., Grueneberg, D.A., Yang, X., et al. (2006). A lentiviral RNAi library for human and mouse genes applied to an arrayed viral high-content screen. Cell *124*, 1283–1298.

Schwarzbauer, J.E., and DeSimone, D.W. (2011). Fibronectins, their fibrillogenesis, and in vivo functions. Cold Spring Harb. Perspect. Biol. *3*, a005041. https://doi.org/10.1101/cshperspect.a005041.

Shiba, Y., Fernandes, S., Zhu, W.-zhong, Filice, D., Muskheli, V., Kim, J., Palpant, N.J., Gantz, J., Moyes, K.W., Reinecke, H., et al. (2013). HESC-derived cardiomyocytes electrically couple and suppress arrhythmias in injured hearts. Nature 489, 322–325. https://doi.org/10.1038/nature11317.hESC-Derived.

Shiba, Y., Gomibuchi, T., Seto, T., Wada, Y., Ichimura, H., Tanaka, Y., Ogasawara, T., Okada, K., Shiba, N., Sakamoto, K., et al. (2016). Allogeneic transplantation of IPS cell-derived cardiomyocytes regenerates primate hearts. Nature 538, 388–391. https://doi.org/10.1038/nature19815.

Tiburcy, M., Hudson, J.E., Balfanz, P., Schlick, S., Meyer, T., Chang Liao, M.L., Levent, E., Raad, F., Zeidler, S., Wingender, E., et al. (2017). Defined Engineered Human Myocardium with Advanced Maturation for Applications in Heart Failure Modelling and Repair. Circulation 135, 1832–1847. https://doi.org/10.1161/CIRCULATIONAHA.116.024145.

Uhlén, M., Karlsson, M.J., Hober, A., Svensson, A.-S., Scheffel, J., Kotol, D., Zhong, W., et al. (2019). The Human Secretome. Science Signaling 12, eaaz0274. https://doi.org/10.1126/scisignal.aaz0274.

Wang, J., Karra, R., Dickson, A.L., and Poss, K.D. (2013). Fibronectin is deposited by injury-activated epicardial cells and is necessary for zebrafish heart regeneration. Dev. Biol. 382, 427–435. https://doi.org/10.1016/j.ydbio.2013.08.012.

Weinberger, F., Breckwoldt, K., Pecha, S., Kelly, A., Geertz, B., Starbatty, J., Yorgan, T., Cheng, K.H., Lessmann, K., Stolen, T., et al. (2016). Cardiac repair in Guinea pigs with human engineered heart tissue from induced pluripotent stem cells. Sci. Transl. Med. 8, 363ra148. https://doi.org/10.1126/scitranslmed.aaf8781.

Wickström, S.A., Radovanac, K., and Fässler, R. (2011). Genetic analyses of integrin signaling. Cold Spring Harb. Perspect. Biol. 3, a005116. https://doi.org/10.1101/cshperspect.a005116.

Zarrinkoub, R., Wettermark, B., Wändell, P., Mejhert, M., Szulkin, R., Ljunggren, G., and Kahan, T. (2013). The epidemiology of heart failure, based on data for 2.1 million inhabitants in Sweden. Eur. J. Heart Fail. 15, 995–1002. https://doi.org/10.1093/eurjhf/hft064.

Ziaeian, B., and Fonarow, G.C. (2016). Epidemiology and aetiology of heart failure. Nat. Rev. Cardiol. 13, 368–378. https://doi.org/10.1038/nrcardio.2016.25.